Modeling circulation patterns induced by spatial cross-shore wind variability in a small-size coastal embayment

Pablo Cerralbo (corresponding autor)

Maritime Engineering Laboratory at Polytechnic University of Catalonia (LIM/UPC),

c./Escar, 6, 08039 Barcelona, Spain

e-mail: pablo.cerralbo@upc.edu, pablocerralbo@gmail.com

Telephone: +34620553942

Manuel Espino

Maritime Engineering Laboratory at Polytechnic University of Catalonia (LIM/UPC) and International Centre of Coastal Resources Research (CIIRC),

c./Jordi Girona, 1-3, 08034 Barcelona, Spain

Manel Grifoll

Maritime Engineering Laboratory at Polytechnic University of Catalonia (LIM/UPC) and International Centre of Coastal Resources Research (CIIRC),

c./Jordi Girona, 1-3, 08034 Barcelona, Spain

ABSTRACT

This contribution shows the importance of the cross-shore spatial wind variability in the water circulation in a small-sized micro-tidal bay. The hydrodynamic wind response at Alfacs Bay (Ebro River delta, NW Mediterranean Sea) is investigated with a numerical model (ROMS) supported by in situ observations. The wind variability observed in meteorological measurements is characterized with meteorological model (WRF) outputs. From the hydrodynamic simulations of the bay, the water circulation response is affected by the cross-shore wind variability, leading to water current structures not observed in the homogeneous-wind case. If the wind heterogeneity response is considered, the water exchange in the longitudinal direction increases significantly, reducing the water exchange time by around 20%. Wind resolutions half the size of the bay (in our case around 9 km) inhibit cross-shore wind variability, which significantly affects the resultant circulation pattern. The characteristic response is also investigated using idealized test cases. These results show how the wind curl contributes to the hydrodynamic response in shallow areas and promotes the exchange between the bay and the open sea. Negative wind curl is related to the formation of an anti-cyclonic gyre at the bay's mouth. Our results highlight the importance of considering appropriate wind resolution even in small-scale domains (such as bays or harbors) to characterize the hydrodynamics, with relevant implications in the water exchange time and the consequent water quality and ecological parameters.

Keywords

Wind-driven circulation, modelling, Bay dynamics, Coastal waters, ROMS, NW Mediterranean Sea, Alfacs Bay, 40.5º-40.7ºN, 0.5º-0.8ºE

1. INTRODUCTION

Tides, winds and freshwater inputs are the main factors determining the hydrodynamics in coastal areas such estuaries and semi-enclosed bays. In micro-tidal and low-freshwater-discharge environments the winds become the main driving mechanisms. The response in bay dynamics to wind forcing has been investigated in detail from different approaches. For instance, Csanady (1973) investigated the current response to a wind in a non-rotating basin, in which the forced response is a surface distortion due to the setup accompanied by a forced flow pattern due to bathymetry variability. Basically, a stable situation shows that in areas shallower than mean water depth the transport is with the wind direction, while it is against the wind direction in deeper areas. Gravitational estuarine circulation is also influenced by winds: intensified with a down-estuary wind, and weakened or even reversed with an up-estuary wind (Valle-Levinson and Blanco, 2004). Furthermore, interaction between wind and gravitational circulation is able to generate substantial transverse circulation in estuaries with a triangular section (Wong 1994), and the influence of winds on exchange flows in narrow areas is demonstrated in Narvaez and Valle-Levinson (2008). Recently, application of 3-D numerical models has allowed the physical mechanisms involving wind-driven circulation in coastal areas to be investigated: for instance, asymmetries in the ebb--flood cycle due to wind forcing in surface layers (deCastro et al., 2003), circulation patterns and water exchange processes (Schoen et al., 2014), and wind model resolution in circulation and wave model behavior (Signell et al., 2005; Klaic et al., 2011; Schaeffer et al., 2011).

Contributions focused on regional and oceanic scales have demonstrated that wind variability due to topographic constraints not only influences the local circulation but also affects mesoscale structures (Chavanne et al., 2002; Jiang et al., 2009). Espino et al. (1998) compares the wind curl with mesoscale circulation in NW Mediterranean Sea, and a theoretical approach to wind curl effects on coastal areas such as the Benguela Current was described by Junker et al. (2015). Zampato et al. (2007) studied the sensitivity of sea level prediction in the Adriatic Sea to different atmospheric model resolution, showing how the finest-resolution models improve the representation of most energetic events. At smaller scales, Rueda et al. (2009) studied the uncertainty of 3-D hydrodynamic models associated with the spatially and temporally varying wind fields in a lake, demonstrating that the better results were obtained using the maximum of available observational data to interpolate the spatial wind fields (reproducing the maximum spatial wind variability). Herrera et al. (2005) studied wind variability on the coast of Spain, emphasizing the wind channeling effects of the Ria de Vigo estuary through a comparison of various meteorological stations. Cerralbo et al. (2012) applied a numerical model in the same estuary and observed that a meteorological model (≈4km resolution) was not able to reproduce all the spatial variability, thus leading to remarkable errors in current modeling. However, only few studies on spatial wind variability have been carried out on bays and estuary dynamics,

mainly due to the lack of meteorological observations and the coarse resolution of meteorological models (on the order of a few kilometers). Klaic et al. (2011) compares the hydrodynamic patterns resulting from the application of different-resolution atmospheric models in the mid-Adriatic, revealing the appearance of new hydrodynamic structures using the finest-resolution models. An interesting example is found in Podsetchine and Schernewski (1999), based on a lake and showing how wind variability on short spatial scales affects the hydrodynamic response. On the other hand, Grifoll et al. (2012) investigated the influence of wind variability in harbors whose layout strongly conditioned the preferential directions for the water motion, thus reducing the effects of the spatial wind variability.

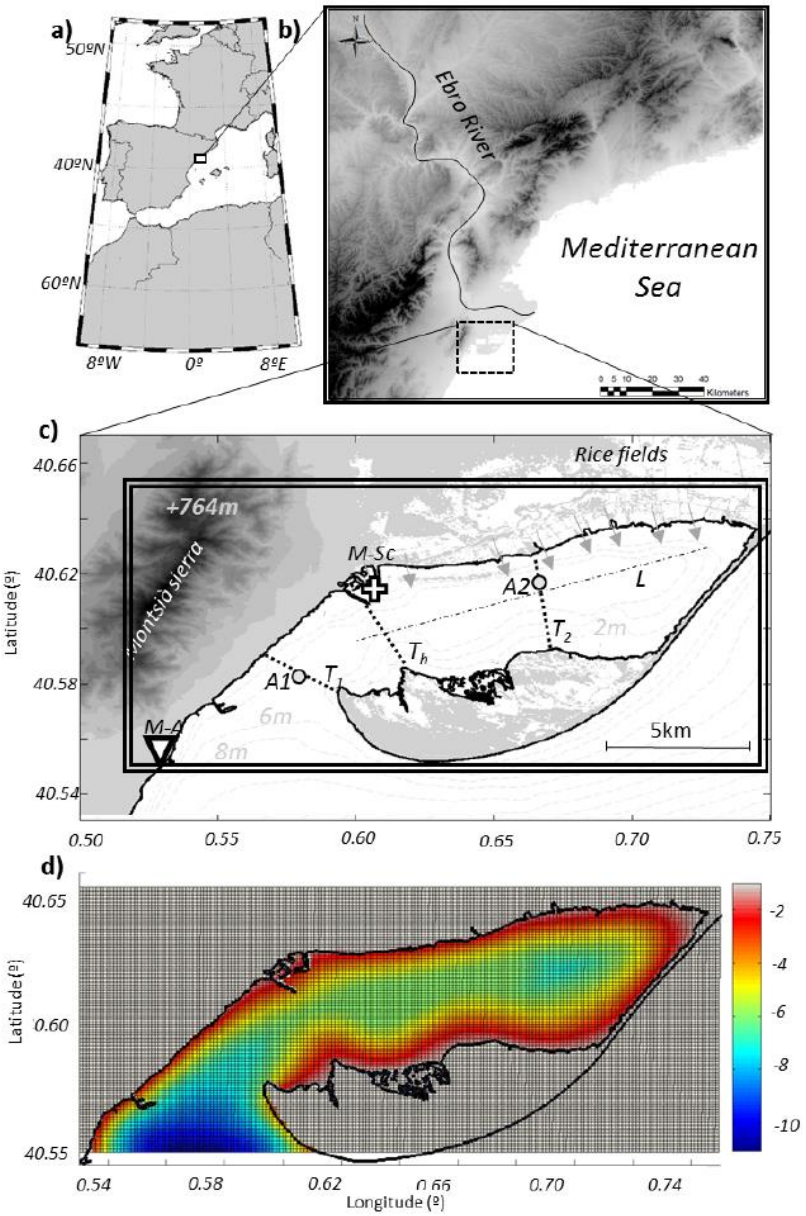

Figure 1. a: Regional location of Ebro River Delta b: Alfacs Bay in Ebro River Delta. c: map of Alfacs Bay. Triangle shows the meteorological station: Alcanar (M-A). White cross for Sant Carles de la Ràpita tide gauge. Gray circles shows ADCP locations (A1 and A2). Dashed lines present crosshore (T_1, T_2 and T_h) and longitudinal (L) section along the bay. Gray arrows on the northern coast shows the freshwater drainage points considered in the simulation. Double line square delimitate the domain for the hydrodynamic numerical model, which is shown in detail in image d (colorbar indicates depth in meters).

The wind variability affects the water exchange between the sheltered waters and the open sea. In this sense, an integrated parameter of water exchange between the bay and the open sea may be also useful to assess the influence of the spatial wind variability on the hydrodynamics. Water exchange time is a physical variable determining how the ecological status of a coastal embayment or estuary is affected by human-induced stresses. For example, short water exchange times indicate that there is insufficient time for the dissolved oxygen to be depleted (i.e. Tweed Estuary, U.K) (Wolanski, 2007). On the other hand, longer times in a restricted coastal area will, potentially, allow an increasing buildup of inputs from land and lead to seasonal or even permanent O_2 depletion in bottom layers and consequently ecological problems (Jickells, 1998).

With the purpose of gaining knowledge of the effects of wind variability in semi-enclosed areas on water circulation, Alfacs Bay (located on the Ebro River delta, Fig.1) was chosen as the study site, where a set of meteo-oceanographic data were available. The main objectives of this contribution are to characterize the hydrodynamic response of the bay under spatial wind variability conditions, as well as to investigate their influence on the water exchange between the bay and the open sea, estimating the water exchange times. The skill assessment of the numerical model is carried out with water current observations obtained during field campaigns in Alfacs Bay. The analysis and discussion of the results are also supported by numerical experiments in idealized domains made in order to investigate the physical mechanism responsible for the hydrodynamic response to the spatial wind variability. Even the results are particularized by the physical characteristics of Alfacs Bay; the new insights provided may be exported to similar domains in terms of hydrodynamic response to heterogeneous wind fields. The paper is organized as follows: the study area, observations and numerical model are described in Section 2. Numerical modeling skill assessment and the results of the numerical experiments are presented on Section 3. In Section 4, we discuss the wind variability effects on the hydrodynamic response and contextualize our results in the state of the art. In Section 5, we conclude by highlighting our main findings.

2. METHODS

2.1 -- Study area:

Alfacs Bay is defined as a bar-build estuary (Pritchard, 1952) formed by the interaction of Ebro River sediment and currents (Fig.1). The bay is around 16km in length by 4km wide, with an average depth of around 4m. The connection with the open sea is 2.5km, with a central channel of 6.5m and shallow shoals of around 1-2m on both sides. The bay is surrounded by rice fields to the north, which spill around $10 m^3 s^{-1}$ of freshwater loaded with nutrients 9-10 months per year into the bay (April-December), and a sand beach closing it on the east side. Monstià Serra, with maximum altitudes of around 700m, closes the bay on the western side (Fig.1).

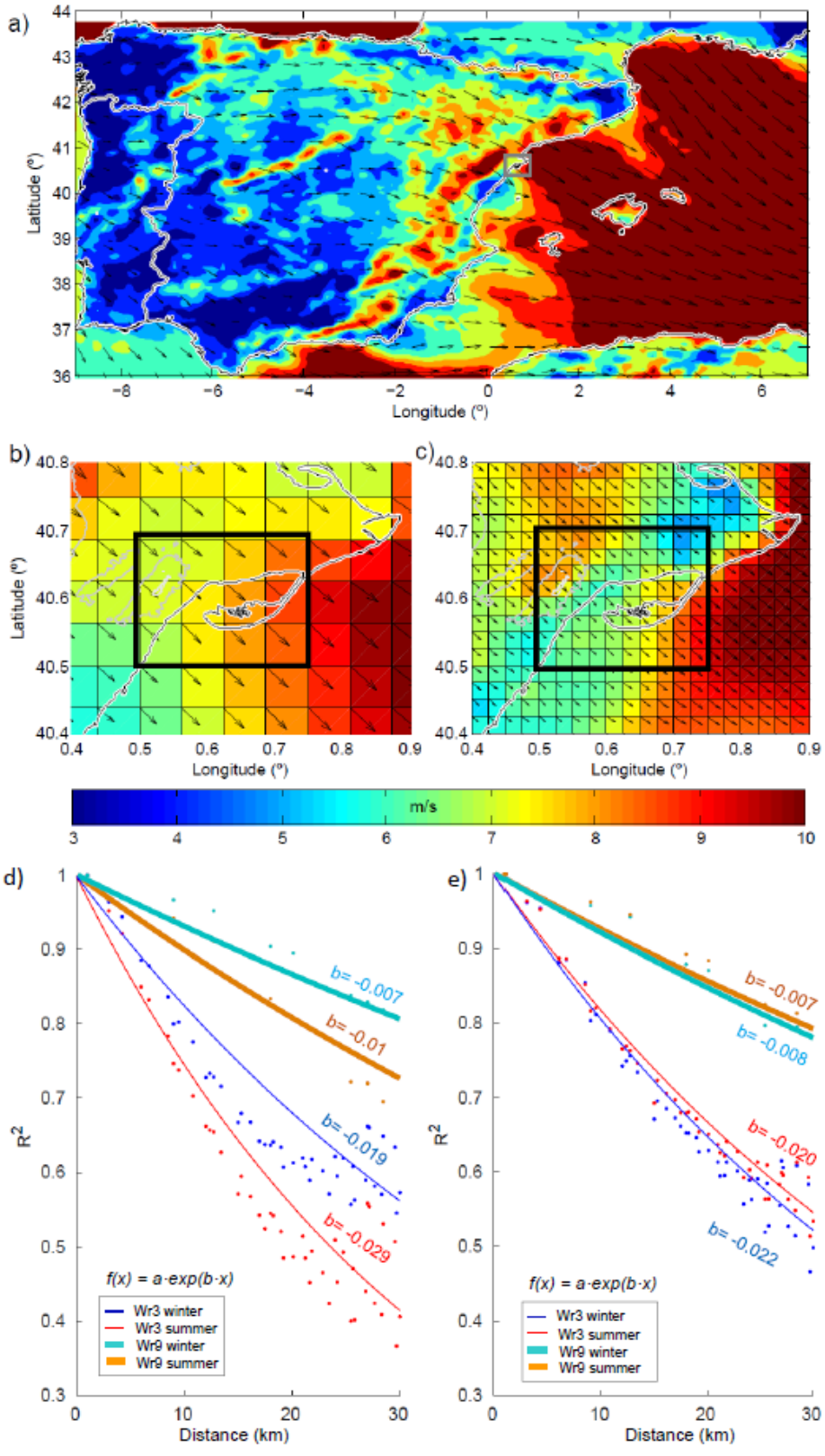

Figure 2. Averaged wind speed and directions for a 36 hours north-western event during 3 and 4th march 2013. Image a) shows regional winds over Spain (WRF9). Grey square delimits the Delta Ebre area. Images b) and c) shows WRF9 and WRF3 configurations in Alfacs Bay. In b) and c) Gray lines shows the contour lines for topography at 200, 400 and 600m. Coastline is plotted in black. Decorrelation scales for eastward (d) and northward (e) wind components for both WRF3 and WRF9 during summer and winter periods.

The bay has been defined as a salt-wedge estuary (Camp and Delgado 1987) with almost stable stratification all year. The highest tidal range during spring tides is around 0.2m, and the hydrodynamic fluctuations are controlled by the wind modulated by the seiche activity (Cerralbo et al., 2014). The most intense regional winds in the area are from the north and northwest (Bolaños et al 2009), establishing a wind jet due to the orographic effects in the Ebro River valley. As an example, 36h time-averaged wind fields (modeled) during a northwesterly event during winter 2014 are shown in Fig.2. In general, the water column used to be stratified due to the freshwater discharge, but well-mixed conditions are more common during winter and mostly related to the hydrodynamic response to wind forcing (Llebot et al., 2013) and occasionally to seiches (Cerralbo et al., 2015a).

2.2 -- Observations:

The bulk of the observational data correspond to two field campaigns: from July to mid-September 2013 and February to April 2014. The data set consisted of water currents from two 2MHz acoustic Doppler current profiler (ADCPs) moored in the mouth (A1) and inner bay (A2) (Fig.1) configured to record 10min averaged data from 10 registers per minute and with 25cm vertical cells. Both devices were equipped with pressure systems and a temperature sensor, and were mounted on the sea bottom at 6.5m depth. Moreover, a chain of three temperature and salinity sensors (CTs) was moored in A2 at around 0.5, 2, and 4m depth, recording minutely data. The sea level data were obtained from the "Catalan Meteo-oceanographic Observational Network" (described in detail in Bolaños et al., 2009) in Sant Carles de la Ràpita harbor (Fig.1) and bottom pressure systems from the ADCPs. Atmospheric data (wind, atmospheric pressure, solar radiation and humidity) were obtained from a fixed land station: Alcanar (M-A) and M-Met (from Meteorological Service of Catalonia, http://www. meteocat.cat).

2.3 – Description of numerical models and simulations:

Numerical wind information was obtained from current implementations of the Weather Research and Forecasting model (WRF; Skamarock et al., 2008) applied at two spatial resolutions (9km and 3km) in Alfacs Bay (Fig.2) and oriented to provide meteorological forecasts by the Meteocat agency. Information, configuration and validation details of the atmospheric models are summarized in Cerralbo et al. (2015b).

The three-dimensional hydrodynamic model used in this study is the Regional Ocean Modeling System (ROMS). Numerical aspects are described in detail in Shchepetkin and McWilliams (2005), and a complete description of the model, documentation and code are available at the ROMS website: http://myroms.org. The implementation of the model consisted of a regular grid of 186 x 101 points with a spatial resolution of 100 m (in both x and y) and 12 sigma levels in the vertical. The bottom boundary layer was parameterized with a logarithmic profile using a characteristic bottom roughness

height of 0.002 m. This value has been considered according to the bottom characteristics of the bay bed (mud and silt as described by Palacín et al., 1991) and the presence of submerged aquatic macrophytes (Camp et al., 1991) and ripples on some areas. The turbulence closure scheme for the vertical mixing is the generic length scale (GLS), described in Warner et al. (2005) and tuned to behave as Mellor--Yamada level 2.5 (k-kl). The implementation included horizontal harmonic Laplacian viscosity and mixing for velocity and tracers, respectively, both with constant coefficients of $5 m^2 s^{-1}$. Future works should determine the importance of these parameters for the validation results for both temperature and salinity in a particular case such as Alfacs Bay. The main configuration values for the model are summarized in Table 1. A two-year simulation (2012-2013) was performed in order to obtain realistic three-dimensional temperature and salinity fields. The sea level and water currents at the boundaries were imposed from hourly sea level data obtained on Sant Carles de la Ràpita, accommodating the perpendicular water velocities at the open boundary axis, consistent with the Chapman and Flather algorithms (Carter and Merrifield, 2007). Temperature and salinity were interpolated from MyOcean products at 6h data (Tonani et al., 2009). Atmospheric forcing and heat fluxes were obtained from M-A (10min) and M-Met. Freshwater inputs were added on the northern coast with an average summer flow of $10 m^3 s^{-1}$ and 0 in winter (Camp et al., 1991). The temperature and salinity fields modeled in the long-term simulations were used as initial and boundary conditions for two simulations coinciding with summer (three months) and winter (one month) field campaigns described in the observations section. For both simulations, open boundary is forced with depth-averaged velocities and sea level measured at A1 (10' data). In summer simulation, freshwater inputs are set equal to $10 m^3 s^{-1}$, whilst in winter simulation they are $0 m^3 \cdot s^{-1}$. For both periods, the skill assessment and validation of the model were done for the sea level, velocities in A1 and A2, as well as temperature and salinity data in A2.

L (number of I-direction rho points)	186
M (number of J-direction rho points)	101
N (number of vertical levels)	12
Hmax (m)	10*
Hmin (m)	1
Baroclinic time step (s)	120
Barotropic time step (s)	40
Bottom roughness (m)	0.002
Dx (=Dy) (m)	100

Table 1. Configuration values used for the numerical simulations

** In the outer bay*

In order to evaluate the hydrodynamic response to wind variability, we designed a set of simulations using different wind fields. Simulation Wr3 used hourly WRF winds at 3km resolution, simulation Wr3-A considered spatially averaged wind values at each time step and simulation Wr9 used wind fields from 9km WRF implementation with a temporal resolution of 3h. The averaged wind values were obtained considering strictly the wind data applied on the inner-bay water surface. We focus on the hydrodynamic response of a six-day period (from 28th February to 6th March 2014), during which northwesterly winds (hereafter NW winds) were blowing in the area (15-20m/s) (Fig.2 shows a 36h averaged wind field during 3rd and 4th March). We selected this period because it shows a series of typical northwesterly events recorded during the extensive campaign period, therefore coinciding with data from A1 and A2. During the northwesterly event, freshwater sources are considered to be equal to $0 m^3 \cdot s^{-1}$, corresponding to rice fields' dry conditions. This period simulation does not consider baroclinic processes in order to isolate the hydrodynamic response to wind variability.

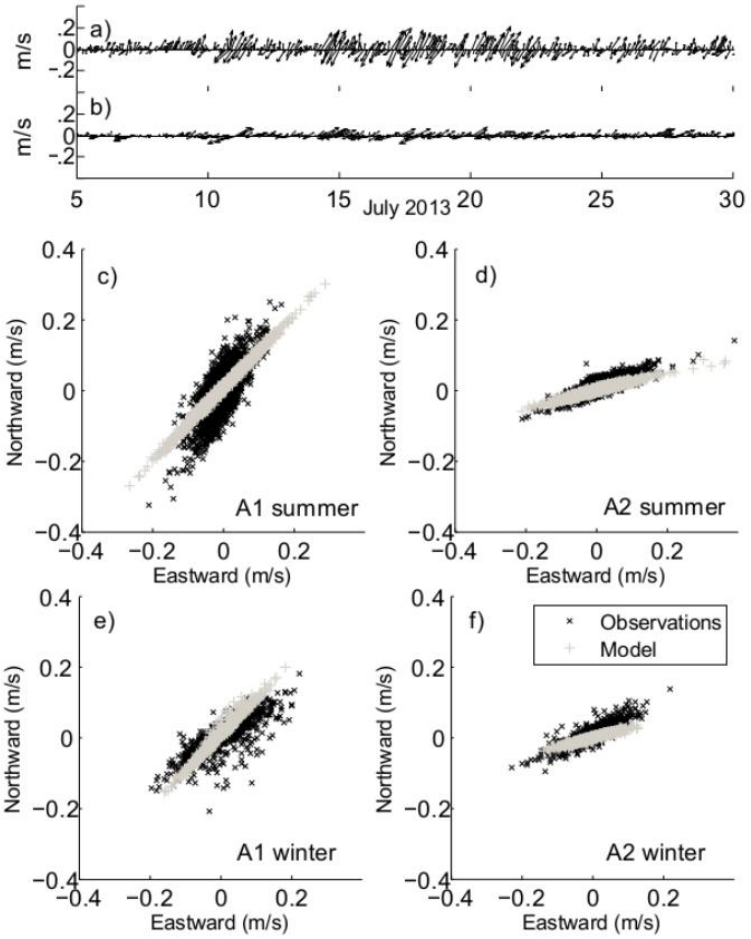

Figure 3. Images a) and b) shows the observed depth-averaged velocities in A1 and A2 respectively during July 2013. Images c) and d) presents the scatter plot on A1 and A2 between eastward and northward depth-averaged velocities for both observational and modelled data during summer 2013. Same for winter campaign in images e) and f).

192 Three cross-sectional sections are defined (T_1, T_h and T_2 in Fig.1) with the objective of describing the
193 role of cross-shore spatial wind variability in the water flows within the bay and open sea. T_1 and T_2
194 coincide with A1 and A2 mooring positions, while T_h represents the narrowest part of the bay's
195 mouth. The cross-sectional flows in each transect are analyzed (positive values indicating direction
196 to the bay's head). Moreover, a longitudinal transect along the main axis of the bay (Fig.1, named L)
197 is utilized to observe the differences in cross-sectional flows. Finally, for the sake of gaining a
198 mechanistic understanding of the bay's response to wind variability, a set of numerical tests in
199 idealized domains are defined, with wind patterns designed to reproduce the observed wind pattern
200 in Alfacs Bay (see Section 2.1) in an idealized shape domain in order to minimize the effects of lateral
201 roughness and nonlinearity induced by irregular bathymetry and coastline. The characteristics and
202 main results are described in detail in Section 4.

203

204 # 3. RESULTS

205 ## 3.1 Model validation

206 The skill assessment of the atmospheric model was presented previously in Cerralbo et al. (2015b).
207 The hydrodynamic model is validated using observational data for summer and winter simulations.
208 Basic statistics (correlation factor and bias) and skill score -- skill assessment index SK (Wilmott,
209 1981) and cost function χ (Holt et al., 2005) -- between observations and modeling results are used
210 to validate the numerical model (see summary in Table 2). SK equals 1 when a perfect agreement
211 between model and observations occurs and decreases to 0 for a complete disagreement. The cost
212 function (χ) is defined as a measure of the ratio of model error to the observed variance. For χ, an
213 acceptable predictive skill of the model is related to values lower than 1 (root mean square error
214 (RMSE) smaller than the standard deviation from observations), and a well-modeled variable
215 threshold is situated at 0.4 (Holt et al., 2005). The aforementioned skill score formulations are detailed
216 in the Appendix. The correlation for sea level during the summer simulation (SS) period is 0.89 and
217 0.85 for A1 and A2, respectively. SK shows values higher than 0.9 and χ close to 0 for both locations.
218 Similar values are obtained for the winter period (WS). In consequence, the agreement for sea level
219 is considered almost optimum.

220 During summer, depth-averaged velocities for the zonal component show correlations of 0.73 (A1)
221 and 0.77 (A2), and values of SK and χ also indicate good agreement (Table 2). The meridional
222 component shows higher agreement at A1 for all skill scores, while at A2 better agreement is observed
223 for the zonal component. The larger correlation in meridional or zonal direction in both places is
224 related to the prevalent alongshore direction due to the bathymetry influence on water circulation
225 (Fig.3c and 3d). Due to the prevalence of barotropic seiche motion, the axis with major variability

corresponds to alongshore directions in both places (Fig.3a and Fig.3b). The scatterplot between observed and modeled depth-averaged velocities showed a significant grade of agreement in both components (Fig.3c, 3d, 3e and 3f). Moreover, there is seasonal variability in the observed--modeled comparison shown in Fig.3c--f. In that sense, due to the most intense seiches being observed during summer (Cerralbo et al., 2014), the modeled currents are overestimated during that period. During winter, the skill scores shows better performance of the model in comparison to the summer period. The correlation for depth-averaged velocities is between 0.8 and 0.9 (with the exception of the northward component in A2).

Table 2. Skill assessment between observed and simulated water currents, sea level, temperature and salinity (summer 2013 and winter 2014)

Variable	Station / Depth	Summer				Winter			
		Bias	r	X	SK	Bias	r	X	SK
Sea Level (m)	A1	0.0004	0.91	0.06	0.93	0.0048	0.91	0.06	0.94
	A2	-0.0058	0.84	0.08	0.91	0.0044	0.89	0.06	0.94
Depth averaged eastern current (m/s)	A1	0.0008	0.73	0.25	0.79	0.0012	0.9	0.06	0.93
	A2	0.0027	0.77	0.14	0.86	0.0023	0.81	0.10	0.88
Depth averaged northern current (m/s)	A1	0.0089	0.84	0.08	0.91	0.0065	0.86	0.11	0.92
	A2	-0.0067	0.62	0.36	0.71	000.33	0.63	0.30	0.57
Temperature in A2 (ºC)	0.5 m	-1.1	0.95	0.5	0.79	-1.80	0.91	0.86	0.71
	2-3 m	-0.89	0.83	0.6	0.77	-1.90	0.91	0.93	0.68
	6 m	0.79	-0.29	1.1	-0.56	-1.70	0.92	1.30	0.67
Salt	0.5m	1.73	-0.20	18	0.0	0.53	-0.20	19.7	-0.007
	2-3m	0.63	0.38	1.60	0.12	0.41	-0.10	31	-0.004

The velocity components are rotated in order to describe the maximum variability in one axis, which is called hereafter alongshore due to its alignment with the central axis of the bay. The main axis is obtained in winter at 36º and 26º counterclockwise for A1 and A2, respectively, and during summer at 59º and 21º for A1 and A2 respectively. The alongshore velocities measured in both A1 and A2 considering vertical variability are graphically compared in Fig.4 with modeling results for both locations and seasons using Taylor diagram (Taylor 2001). In this diagram, the comparison between observations and the model are shown in terms of correlation, the centered root mean square difference (CRMSD) and the standard deviations (see Appendix). Along-shore correlations ranges

between 0.6 and 0.7 for both locations (SS and WS), whilst cross-shore show values lower than 0.4 for all layers. In order to compare in the same figure different vertical layers against observations, the standard deviations and CRMSD are normalized over the standard deviation of the corresponding observations (Grifoll et al., 2013). In the diagram, the model skill improves as the points get closer to the observation reference point. The proximity of A1 to imposed boundary conditions induces better agreement than A2, where the role of bay dynamics (stratification or nonlinearity induced by bottom friction) is complex and modifies the water response. On the other hand, during winter (WS) all the skill scores indicate better modeling performance than summer, probably due to the discrepancies in the modeled stratification (higher during the summer period). Future experiments using spatially variable bottom roughness should be conducted in order to understand the importance of such variability in the water currents.

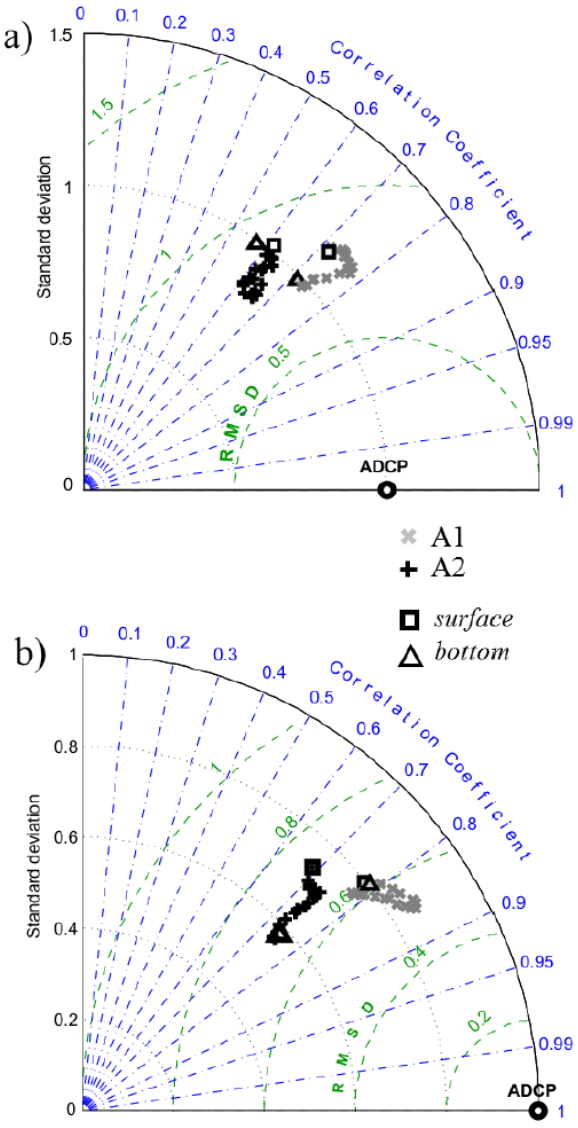

Figure 4. Taylor diagram illustrating the match of modelled along-shore velocities in A1 (grey) and A2 (black) to its corresponding observational data. Summer 2013 on (a), and winter 2014 in image (b). Both model and observational data are averaged in vertical layers of 25cm.

Modeled temperature is compared with CTs and ADCP sensors, revealing a high correlation and good skill assessment factors for inner-bay (A2) surface sensors. At 3m depth, the correlation is still good albeit lower than at the surface. However, during summer, on bottom layers the correlation is close to 0, indicating no agreement with observational data, whilst during winter the modeled bottom layer temperature follows the observational data. The processes that lead to discrepancies in these layers during summer may be related to differences in the mixing processes in the water column. The differences observed from the surface to the bottom are around 2ºC for almost the entire summer, while the model reveals differences of about 0.5ºC. The bias shows how that model underestimates the temperature during summer and winter. However, the skill scores show good behavior, because the period and magnitude of the diurnal oscillations are well reproduced by the model. Maximum RMSE is around 1.3 ºC and similar to previous modeling works at Alfacs Bay (Llebot et al., 2013).

Finally, salinity data were only available for the beginning of the summer campaign (around 15 days) due to biofouling. Moreover, in winter, the sensor at 4m did not work properly during the whole campaign. During summer, the differences between 3m and surface salinity were around 1.5 in A2, while in the model these differences were around 0.3--0.4. The discrepancies of the numerical results and the observations seem to indicate the presence of other sources of freshwater fluxes (i.e. groundwater fluxes or an increase of continental runoff not monitored) and a possible overestimation of the mixing. Sensitivity tests using double and quadruple freshwater flows during summer show remarkable differences in salinity and temperature values along the bay. These results indicate the relevance of a detailed information of freshwater inputs, thus encouraging future studies to address and rectify this lack of information considering also potential contribution of fresh groundwater sources (Camp, 1994). During winter, the salinity bias in both 0.5m and 2m layers was lower, albeit still positive, indicating higher simulated than observed salinity values. This agrees with previous studies that observed that during winter, even with the drainage channels closed (no water in rice fields), the bay still received freshwater inputs (lower salinity than open sea) (Camp and Delgado 1987).

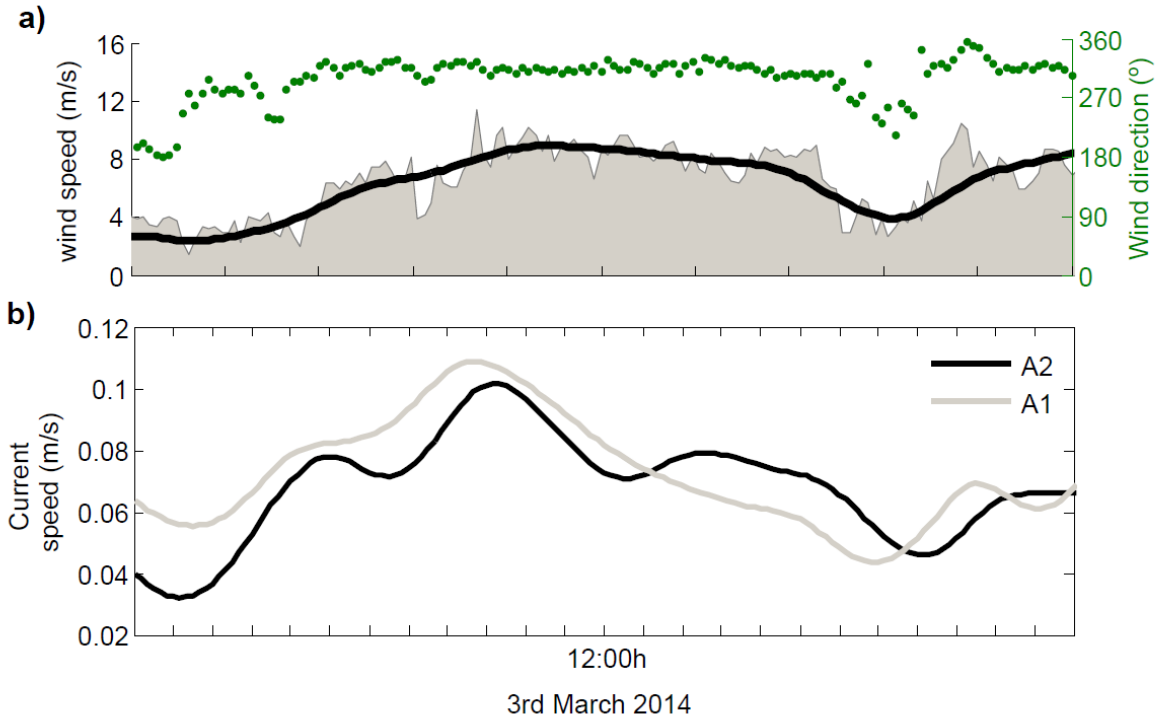

Figure 5. a) Wind measurements on M-A during 3rd March 2014. Grey area sows wind speed observations, and black thick line for 6h lowpass-filtered data. Green dots for wind direction. b) Current speeds measured at surface (1m averaged layer) on both A1 (gray) and A2 (black), filtered with Lanczos lowpass filter of 6h.

283

284 ## 3.2. Hydrodynamic response to wind variability

285 The hydrodynamic response is investigated in detail during the northwesterly wind event for the three
286 simulations suggested in Section 2.3. In this period, the winds were blowing mostly from the north
287 and northwest, lasting for more than 12h with sustained wind speeds higher than 8 $m \cdot s^{-1}$ (Fig.5a) and
288 maximum wind gusts of 20 $m \cdot s^{-1}$. Time-averaged winds for 3rd and 4th March showed noticeable
289 spatial variability in Alfacs Bay (Fig.2a-c). One way to quantify the spatial variability is through the
290 decorrelation distance. Using all the data inside the area marked in Fig.2b and c, the decorrelation
291 scale is obtained for both periods, analyzed by components and then adjusted with an exponential
292 equation (Fig.2d and 2e). Results show clear differences between WRF at 3km and 9km, revealing
293 that the correlation decays much more clearly at smaller length scales with WRF at 3km, thus
294 indicating that higher-resolution products resolve more spatial features. Moreover, differences
295 between the summer and winter period reveal more variability during summer, probably related to
296 the presence of more locally influenced wind sea breeze. These gradients were also appreciated at
297 shorter timescales. For instance, Fig 6.e1 shows a snapshot of the wind fields at 10:00 UTC on 3rd
298 March (corresponding to simulation Wr3). Maximum velocities are observed in the inner area of the
299 bay, with an almost calm region over the bay's mouth. This picture agrees with the wind pattern for

NW described in Cerralbo et al. (2015), suggesting wind shadowing effects from local and regional orography on some occasions. The wind pattern shows a transition zone with maximum wind intensity gradient between T_h and T_2 sections. The averaged wind field (Wr3-A) presented intensities of around 6 $m \cdot s^{-1}$ from the NW (see snapshot in Fig 6.a1).

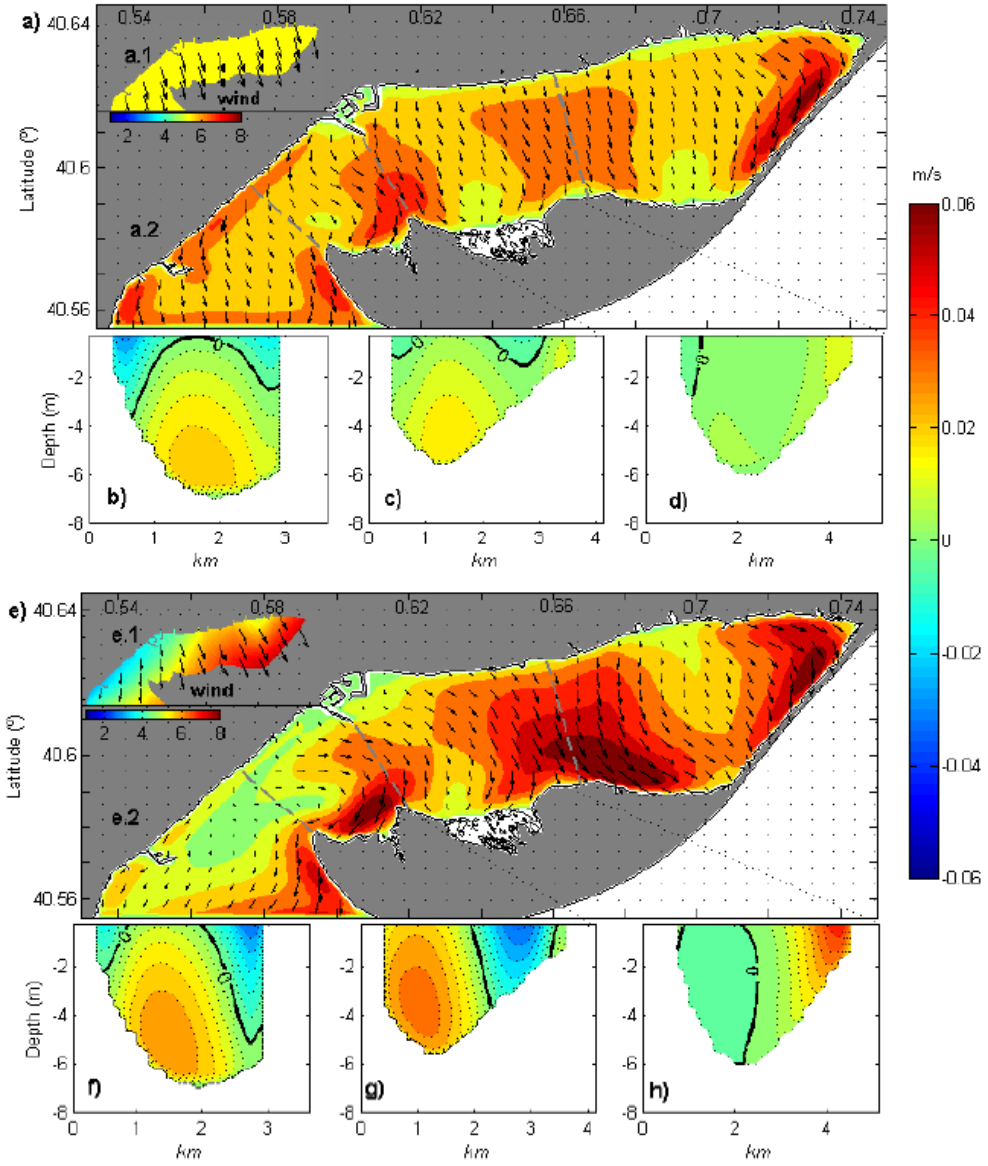

Figure 6. Results corresponding to 10:00h UTC 3rd march.Wr3-A experiment in *a* to *d* images. Wr3 in *e* to *h*. Images on the top left corner of a and e (a.1 and e.1) shows snapshot of wind forcing ($m \cdot s^{-1}$) in each experiments, while big size images (a.2 and e.2) show surface currents modelled with ROMS. Images *b* and *f* for cross-sectional velocities along T_1, *c* and *g* for T_h and *d* and *h* for T_2. The initial point for each transect (km 0) is located on the northern shoal. In *a* and *e*, colors for wind and current speeds (different scales). In cross-sectional plots, colors represent velocities: positive values indicating inward bay velocities, and negative for outward water currents.

The modeled water circulation for Wr3-A (Fig.6a) shows mean surface velocities around 4-5 $cm \cdot s^{-1}$, with surface currents following the wind direction. The maximum intensities are observed in the narrow areas and coincide with headlands in the southern margin of the bay. In the eastern margin,

the shoreline and the shallow bathymetry force the alignment of the currents with the boundaries. A similar current pattern but larger water velocities are modeled for the Wr3 simulation. The most intense currents for Wr3 are obtained in the inner bay, according to higher wind stress. At the bay's mouth, surface velocities in Wr3 are lower in comparison to Wr3-A, coinciding with areas with the lowest wind stress. Noticeable variations in surface water direction are observed at the bay's mouth (between T_1, T_h and offshore). In this area, the water current is intensified on the southern side of the mouth, and a counter flow towards the inner bay appears on the northern side.

The corresponding cross-sectional currents for the three sections considered (i.e T_1, T_2 and T_h) are presented on Fig.6b--d and f--h. Positive means inward flow, and negative means outward flow. For transect T_2 in Wr3-A velocities across the section are small and the flow is positive (inwards). For Wr3, larger velocities induced by wind stress over the eastern margin and southern shore induced a significant increment of inward flow in T_2 (south extreme). For this section, outward flows occupy half of the section, with horizontal shear in the along-shelf direction. Alongshore currents for T_1 section show a similar pattern between Wr3 and Wr3-A simulations, with outward flow over margins and inward flow in the deep central channel.

The most relevant differences between numerical tests appear on the T_h transect. For Wr3-A water circulation follows the main wind direction in the surface layers, with a divergence flow in the southern headland. On the other hand, for Wr3 this section coincides with the vertex of an anti-cyclonic gyre observed between T_1 and T_h. Alongshore velocities through sections reveal structures completely different between both tests. For Wr3-A, horizontal shear is observed between the margins (outward flow) and the central area, along with vertical shear in the margins, with ingoing flows at the bottom (Fig.6c). On the other hand, Wr3 reveals a clearly horizontal two-layered structure (no vertical shear), with inflows in the northern region and outflow in the south (Fig.6g). The intensities of these flows are much higher than Wr3-A.

To explore the vertical structure of the flow along the bay and with the same wind direction (almost cross-shore), the velocities across transect L (Fig.1) are shown in Fig.7, corresponding to the same instant as Fig.6. Both numerical simulations show a two-layered vertical structure, with surface currents flowing downwind (negative values), and a northwestward return flow (upwind, positive) in the deeper layers. The bottom circulation shows two regions of maximum velocities: one region between T_h and T_2 and another between T_2 and the eastern boundary of the bay. These regions are also observable in Fig.6a, showing lower surface velocities linked with the return flow observed in the bottom circulation. Differences between Wr3 and Wr3-A yield different water velocity of upwind and downwind flows. In particular, larger intensities are found for the Wr3 simulation in comparison to Wr3-A around T_2.

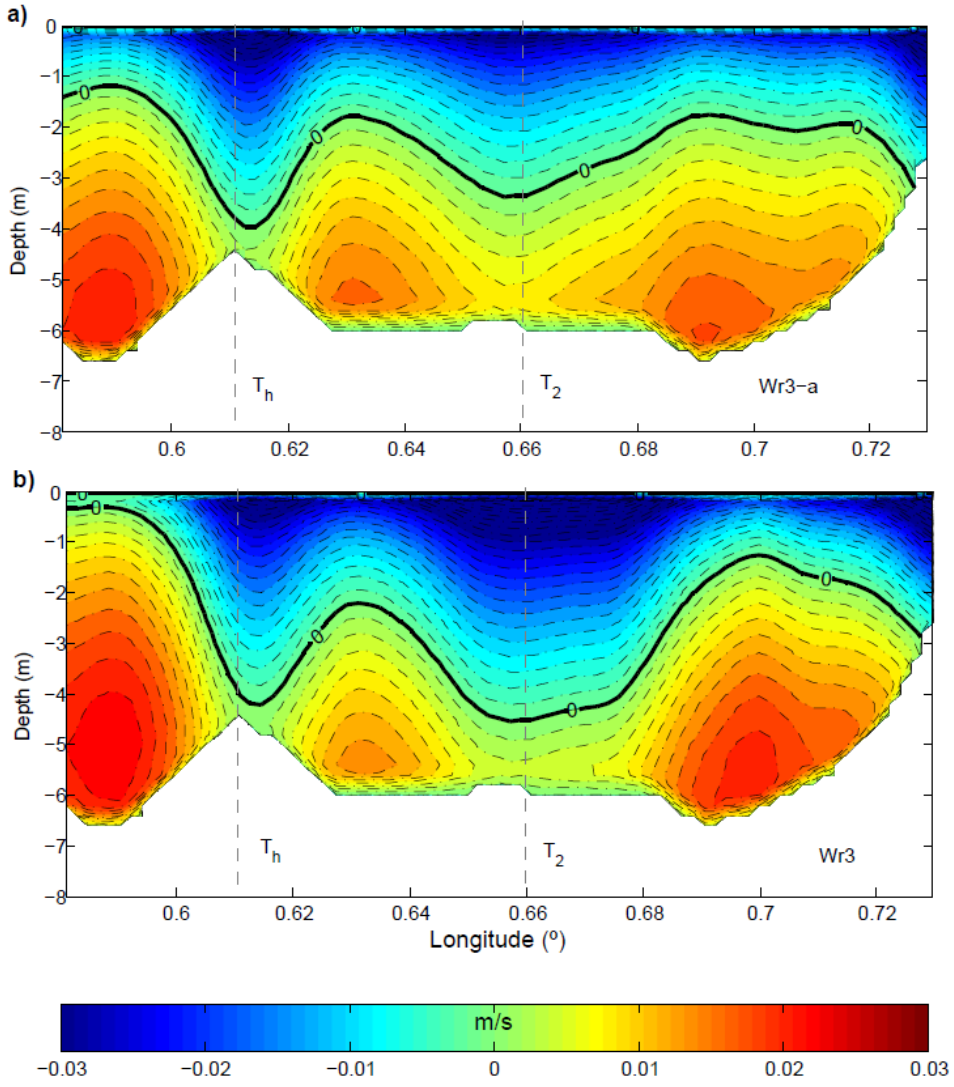

Figure 7. Cross-sectional velocities along L section (Fig.1) for both Wr3-A (a) and Wr3 (b) numerical tests. Positive values for velocities northward, and negative values for velocities shouward. The location for sections T_h and T_2 are marked with dashed lines.

341

342 The temporal evolution of net exchange flow over each cross-shore transect is obtained for the entire
343 northwesterly event in both Wr3 and Wr3-A simulations. The inflow differences between simulations
344 (Wr3 minus Wr3-A) are plotted in Fig.8b, c, and d. The mean, standard deviation and total flow
345 differences throughout each section are summarized in Table 3. Differences in T_2 and T_h sections are
346 evident, with an increase of net flow (positive) for Wr3 simulation in comparison to the Wr3-A case.
347 In contrast, the T_1 section does not present significant differences for both simulations. Standard
348 deviations reveal similar values for the three sections. These differences could also be defined in
349 relative terms (percentages of variation). In this case, the Wr3 case versus Wr3-A represents an
350 increase of 14 and 22% of mean flows through sections T_2 and T_h, respectively, and a decrease of
351 around 3% in T_1. The dashed box in Fig.8 corresponds to the snapshot plotted in both Fig.6 and Fig.7.

For both T_h and T_2 this event is related to a period of significant maximum (positive) differences. During this snapshot the flow differences between simulations for T_1, T_2 and T_h were 41, 44 and 88 $m^3 \cdot s^{-1}$, respectively, computed from the cross-sectional flow shown in Figure 6. The previous numerical results reveal a strong influence of the wind direction in the vertical structure of the flow (Fig.6).

Table 3. Statistics from flow differences in each transect (WRF3 - $WRF3_{avg}$) from 28 February to 5th march 2014.

Section	Standard Deviation	Mean (m^3/s)	Total (m^3)
T_1	16.34	-2	$- 9.68 \cdot 10^5$
T_h	19.17	+13.6	$+ 68.96 \cdot 10^5$
T_2	17.73	+12	$+ 65.02 \cdot 10^5$

A hydrodynamic time parameter applied to the defined volumes is used to analyze and compare the flows due to wind variability and their relative effects on the water exchange in Alfacs Bay. There are many definitions used to describe the hydrodynamic time parameters for a given domain, the simplest one being the ratio of total volume (V) to water flow (Q) entering or leaving it (Jouon et al. 2005). The methodology is based on the displacement concept, which gives us the time required to displace all the water in a volume once, assuming that all water particles have the same transit time through the control volume. This means that, when using this approximation, space and time variability of the hydrodynamics within the control volume is not considered. This is summarized in $\theta = V/Q$ (with θ as water exchange time) as proposed by Jouon et al. (2005). Following the bay division presented in Fig.1 by T_1, T_2 and T_h, we used the cross-sectional flows and corresponding water volume enclosed on their eastern side or inner-bay side (naming each volume as V_{T1}, V_{T2} and V_{Th}). Results for the entire northwesterly wind event are presented in Table 4. With non-variable winds (Wr3-A) the highest flow appears in T_2 (biggest section, with $16.4 \cdot 10^3$ m^2, and around $15 \cdot 10^3$ m^2 in T_1), almost twice that observed in T_1 and T_h. Considering the volume of water enclosed by each section, the θ shows similar values for both T_1 and T_h and minimum ones for T_2. Considering the wind variability, the averaged flows and corresponding θ are modified in T_2 and T_h, reducing them about 14% and 20% respectively, and remaining without noticeable changes at T_1. On the other hand, the hourly snapshot observed during 3rd March at 10:00 UTC (Fig.6 and 7) reveals noticeable variations in all the sections, showing associated water exchange time reductions of 20%, 47% and 40% for T_1, T_h and T_2, respectively, between Wr3 and Wr3-A.

Table 4. Statistics from flows on sections T_1, T_2 and T_h from 28 February to 5th march 2014 (represented by mean values). The water exchange times (θ) are computed considering the area they have on the east side (Fig.1).

T	Volume ($x10^8$) m^3		Q_{mean} ($m^3 \cdot s^{-1}$)	θ (days)
T_1 (V1+Vh+V2)	2.44	Wr3	53.16	53
		Wr3-A	55.07	51.3
T_h (Vh+V2)	1.99	Wr3	58.8	39.2
		Wr3-A	45.9	50.2
T_2 (V2)	1.06	Wr3	99.47	12.3
		Wr3-A	85.9	14.3

4. DISCUSSION

Current measurements have shown the complexity of the water circulation due to the nonlinearity of the flow and the non-stationary response. This behavior is related to the short frictional time adjustment (estimated to be 1.5h according to Cerralbo et al., 2015a) and short sea level adjustment time at wind forcing. A linear response to wind forcing is only expected during the first hours of wind events. For instance, during 3rd March (northwesterly event) the current velocity measured in A1 and A2 increases at the same time as the wind intensity (see Fig.5). Then, after a few hours, although the wind intensity remains approximately constant, the velocity of the surface currents decreases due to the likely adjustment of the frictional effects as well as the emergence of other terms in the momentum balance (i.e. pressure gradient and advective term). For instance, the adjustment time for the appearance of sea level gradients is on the order of the length of the bay divided by the celerity of long gravity waves ($\sim(g \cdot H)^{1/2}$). Applied at Alfacs Bay the adjustment time is around 50min. Therefore, for periods of a few hours it is realistic to consider the wind setup (i.e., 1cm with winds of around $10ms^{-1}$ and assuming bay width of 4km) opposing the wind stress. For longer periods, the sea-surface adjustment time may lead to the generation of longitudinal and lateral oscillations as well as internal seiches in the bay due to the transient nature of the wind, variability in the remote sea level forcing (e.g. atmospheric pressure; Boegman, 2009) or stratification. Moreover, the differences in water column stratification could imply significant differences in surface water response to wind stress. For instance noticeable differences in the stratification of the water column between the inner bay (mixed) and bay's mouth (stratified) were observed on 25th February (Cerralbo et al., 2015a). In consequence, the expected larger water velocities in A2 in comparison to A1 due to the wind variability during the northwesterly wind event are partially hidden by the complex response of the bay.

Due to the lack of additional meteorological and hydrodynamic observations within the bay to complete the analysis of the wind variability response, the results of the validated modeling system

(atmospheric and hydrodynamic) provided interesting insights. Previous works in Alfacs Bay (Camp, 1994; Llebot et al., 2013) have observed well-mixed conditions in winter under energetic cross-shore winds. In addition, observations only one week before the northwesterly event showed complete water column mixing in the bay (Cerralbo et al., 2015a). In consequence, in order to isolate the hydrodynamic wind response, the stratification and the astronomical tides have not been considered in our simulations.

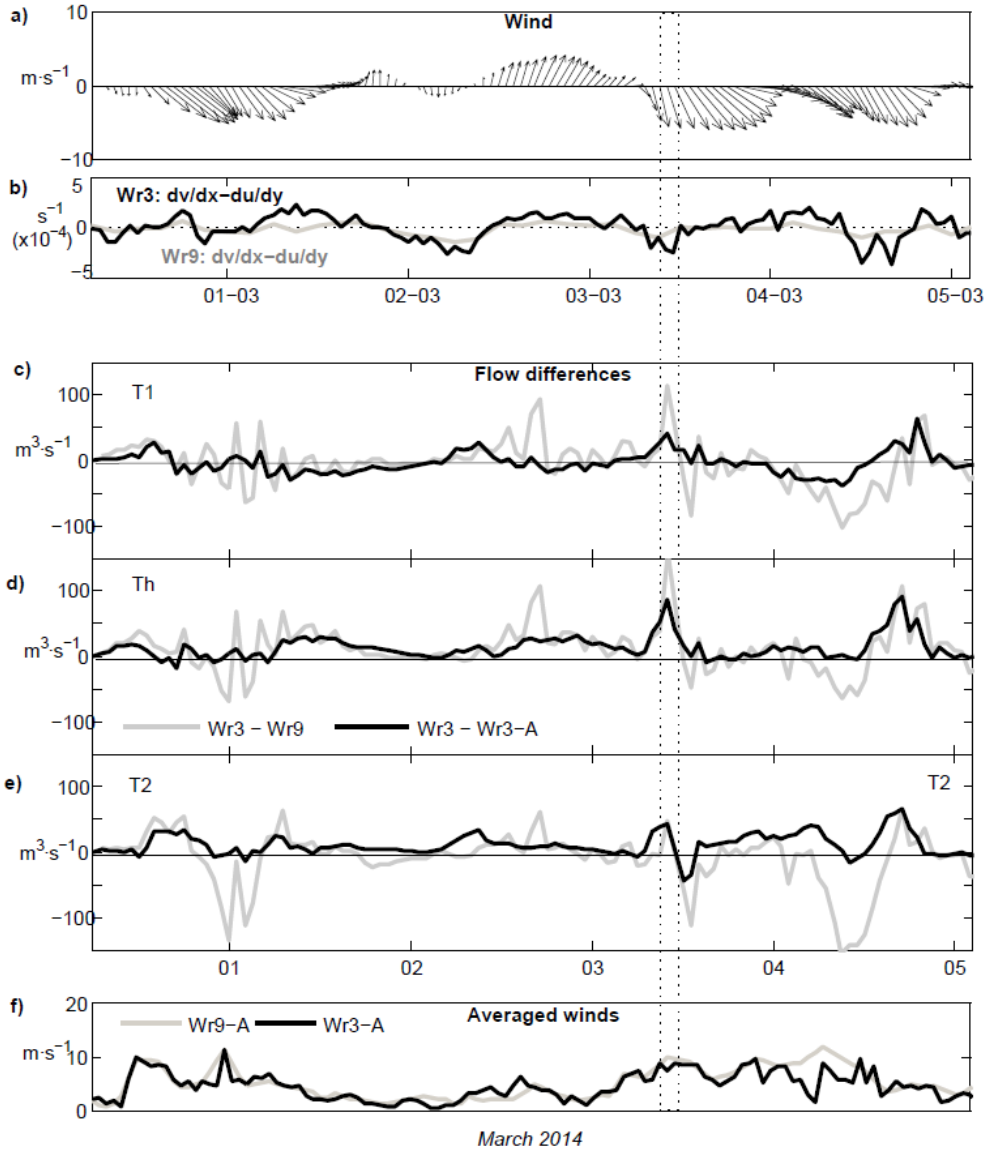

Figure 8. a) Spatial averaged winds for Wr3 (and Wr3-A) between 28 February and 6 March 2014. The wind has been filtered using low pass band filter (Lanczos) of 2h. b) Averaged vorticity for Wr3 over the domain marked with black line in Fig.2b. Images c, d and e) black thick line shows the flow difference through each section (corresponding panel) between Wr3 and Wr3-A numerical tests (Wr3 minus Wr3-A). The flows are for the corresponding hourly snapshot. Grey line shows the difference from Wr3 to Wr9 tests (Wr3 minus Wr9). Image f shows the spatial averaged wind speeds over the domain marked with black line in Fig.2b and 2c for both Wr3 and Wr9 in black thick and gray lines respectively.

Numerical simulations using cross-shore spatial wind variations (Wr3) versus the homogeneous case (Wr3-A) reveal noticeable differences in hydrodynamic structures. One of the most noteworthy hydrodynamic features observed is an anti-cyclonic gyre close to the bay's mouth. This structure is clearly observable in Fig.6 and Fig.7b and is related to an increase of the flow between T_h and T_2. The water fluxes through the sections (summarized in Table 3 and Fig. 8) show that the wind variability not only determines the hydrodynamic response but also affects the water fluxes through the bay. A similar structure at the bay's mouth is found 24h later (not shown). Sectional flow differences between numerical simulations showed two clearly different hydrodynamic responses: T_h and T_2, with noticeable differences between tests, and T_1, revealing lower sensitivity to the wind variability. Therefore, the wind variability in inner areas (T_h and T_2) implies noticeable reduction of water exchange times. However, these differences among spatially variable (Wr3) and non-variable (Wr3-a) winds in T_h and T_2 respond to different physical mechanisms. Over T_2 the differences are due to an increase of wind speed (Wr3-A to Wr3) affecting the circulation pattern (quadratic effects through wind stress). Otherwise, over T_h (and T_1) the wind is much lower in Wr3 than Wr3-A, and in this case the mechanism that leads to the flow increment is related to the appearance of the anti-cyclonic structure.

In order to understand the mechanism which leads to the hydrodynamic pattern observed in Fig.6 and Fig.7, a set of idealized numerical tests were implemented. The geometry is reduced to a rectangular shape (oriented east--west) opened at the southwestern side with a north--south- oriented channel keeping away the open boundary (Fig.9). Reference test is forced by $5 m \cdot s^{-1}$ northwest wind (Fig.9a). The wind variability tests are defined by a zone with constant winds of $2\ m \cdot s^{-1}$, and then wind speed is increased linearly towards the eastern side. Wind patterns along the x-axis are defined above each image in Fig.9. Two experiments, with the region of varying wind occupying 2/3 or 1/3 of total area, were designed (Fig.9c-d and e-f, respectively). Another test with extreme variations is presented in Fig.9g-h; in this case the region of constant wind is defined as $0 m \cdot s^{-1}$. The spatially integrated wind intensity is the same for all cases and equivalent to $5 m \cdot s^{-1}$ over each grid in the homogeneous test (Fig.9a). The same geometry and numerical mesh are used with two different bathymetries: flat bottom with 4m water depth and bathymetry with shoals of 2m depth in the lateral margins and a central channel of 6m (see Fig 9b). The model implementation is the same as the realistic case presented in Section 2, except that the water density is homogeneous in the whole domain. The numerical solution is analyzed after 24 hours of simulation, when the stationary conditions are reached. For flat bottom with homogeneous wind fields (Fig.9a), the surface currents move in the same direction as the wind (+3º clockwise from winds). For the channel bottom case, surface currents are modified in comparison to the flat-bottom case (Fig.9b).

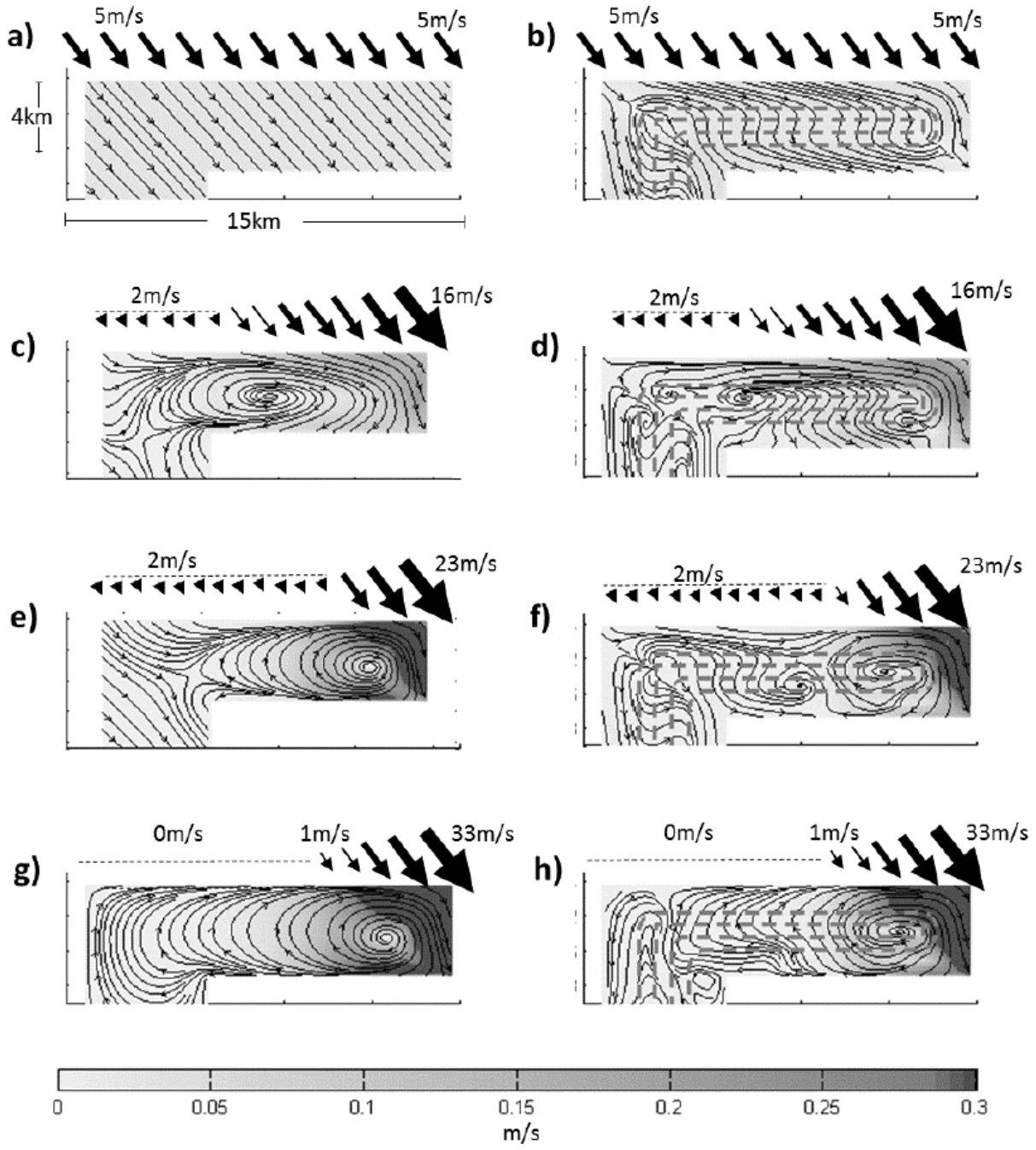

Figure 9. Surface streamlines for idealized schemes. Each panel shows the velocity module contours (grey scale) and streamlines for each of the idealized wind tests after 24hours of simulation. The winds along x-axis utilized in each test are shown at the top of each panel. Left images for flat bathymetry (4m depth) and right images for channelized bathymetry. Isobaths 4m and 6m are plotted in dashed grey lines in image b, d, f and h.

Over the shoals the currents flow with the wind direction but are rotated 30º counterclockwise, while in deeper areas (central channel) the surface currents rotate 45º clockwise. Cases c and d are similar to the wind described in Fig.2 and Fig.6 but with larger wind gradients. The eastern corner shows the highest water velocity with a similar direction to wind forcing, whilst over the region with lower wind speeds high variability in water surface currents appears. A similar structure (gyre) described in Fig.6

appears in the transitional wind area. When the wind gradient is applied more to the east (Fig.9e and f), a clear anti-cyclonic gyre is also observable but located in the innermost area of the bay. The last case (with no wind on the west side) maximizes the effects of the anti-cyclonic gyre. The southeastward currents induced by wind pull water from the areas with no wind. Then the anti-cyclonic gyre is established covering the entire width of the bay. This gyre is observed in all the experiments with wind variability (with both types of bathymetries). The results from idealized tests indicate that the water circulation on the left side of the wind gradient is characterized by a gyre. The responsible mechanism is the wind curl, establishing an eastward surface current in the northern region of the bay with calm winds, and westward flows in the southern regions. Although the bathymetry has been idealized through a central channel, the numerical results show that the cross-shore wind variability dominates over the bathymetric effects under these circumstances. Therefore, in our idealized case the spatial wind variability is at least as important as bathymetry in driving the circulation.

At larger spatial scales than Alfacs Bay, several authors have observed that the vorticity of wind fields is related to the generation of mesoscale gyres (eddies) on more regional scales such as the Mediterranean Sea (Espino, 1997; Schaeffer et al., 2011) and the Hawaii Islands (Chavanne et al., 2002). However, the gyres and vortices modeled in Alfacs Bay related to wind variability are not usually described in small coastal embayments (characteristic length of 10km). The spatial mean wind curl ($\frac{\sum_{i=1}^{n}\left(du/dy - dv/dx\right)}{n}$, with n for each data pixel) from Wr3 (domain in Fig.2) is shown in Fig.8b for the northwesterly event. The highest negative values coincide with northwesterly wind events and respond to the wind variability shown in Fig.2 and Fig.6. Results indicate that negative vorticity close to T_h is causing the appearance of the anti-cyclonic gyre observed in Fig.6 and described in the idealized tests (Fig.9). In Alfacs Bay, during most energetic winds, the entire water column would respond to wind stress -turbulent boundary layer larger than the maximum water depth (Llebot et al. 2013, Cerralbo et al. 2015a)- proving the importance of an accurate description of spatial wind variability.

The averaged flow and timescales in Alfacs Bay are investigated in order to analyze the influence of spatial wind variability over the entire northwesterly event. Camp (1994) uses salinity-balance-based approximation to obtain the water exchange time as V/Q, albeit considering the estuarine circulation as the flow through the section. In his case, a flow of $150 m^3 \cdot s^{-1}$ and $40 m^3 \cdot s^{-1}$ through a similar section of T^h during open- and closed-channels seasons, respectively (corresponding to water exchange times of 14 and 50 days), was obtained. Even these flows are an approximation, and they respond to a completely different physical forcing (gravitational circulation) from what we have used: they gave us an idea of temporal (θ) and velocity scales (flows) in the bay. When comparing these values with

483 the numerical results during northwesterly event, it is clear that during the closed-channels season
484 (winter) the role of the wind variability in the bay exchange flows must be considered (Wr3 and Wr3-
485 A show flows of 59 and 46 $m^3 \cdot s^{-1}$, respectively).

486 For the northwesterly event we have applied the WRF model at 9km resolution (Wr-9) to assess the
487 results using medium-range products of meteorological forecasts. The averaged wind field is shown
488 in Fig.2a. The flow differences between Wr3 and Wr9 are summarized in Fig.8c, d and e (grey line).
489 In general, their differences are similar to the ones observed between Wr3 and Wr3-A. The correlation
490 between flow differences from Wr3 to Wr3-A or Wr9 moves from 0.56 in T_1 and to 0.67 in T_h,
491 indicating that the numerical resolution used in Wr9 is equal to Wr3-A and does not reproduce the
492 spatial variability under some circumstances. The spatially averaged velocities for both Wr3 and Wr9
493 are shown in Fig.8f, revealing that the differences between them are minimum most of the time; under
494 some circumstances (i.e. 1st and 4th March) Wr9 is even more intense. These differences imply a flow
495 increase through the sections. Moreover, it has been demonstrated that these high-resolution models
496 are able to solve spatial structures (not reproduced by coarser models), which implies noticeable
497 variations in hydrodynamic structures, as observed in Klaić et al. (2011) and Zampato et al. (2007).
498 In consequence, in this contribution case we only estimates hydrodynamic differences explained by
499 wind curl but energetic differences may be also raised from different wind resolution products. On
500 the other hand, Wr9 has a temporal resolution of 3h. Considering that the time response of Alfacs
501 Bay is on the order of a few hours, we can expect that models with larger time resolution would imply
502 loss of relevant information (for instance, in the exchange flows; see Fig.8). Future research will
503 include studies on temporal resolution impacts on hydrodynamic response.

504 For stratified conditions in the water column, larger velocities in the surface layer are expected due
505 to the diminishing of the vertical momentum transfer. However, observational studies and numerical
506 sensitivity tests show that the stratification is modified by energetic NW wind events (Llebot et al.,
507 2013; Cerralbo et al., 2015a). During these events the wind stress is able to mix, and the circulation
508 pattern obtained by the homogeneous case is reproduced in the stratified-water-column simulations.
509 Therefore, despite the limited depth of Alfacs Bay and the reported stratification due to freshwater
510 and heat fluxes, we assume that the response pattern to wind variability would not vary significantly
511 under most energetic winds described in this contribution. However, spatial variability in weaker
512 winds under stratified conditions would promote more complex circulation. The response under
513 weaker winds will benefit from extended and simultaneous stratification and water currents
514 observations.

515 Several contributions in similar domains to Alfacs Bay (i.e. shallow and micro-tidal environments)
516 have investigated the hydrodynamic response using homogeneous winds: for instance, Cucco and

Umgiesser (2006) at the Venice Lagoon (Italy), Ferrarin et al. (2010) at Marano and Grado (Italy), Alekseenko et al. (2013) at the Berre Lagoon (southern France) and Schoen et al. (2014) at an estuarine lake in South Africa. Also the hydrodynamics of large harbors have been investigated based on wind measurements at one point (Mestres et al., 2007; Grifoll et al., 2011). Finally, Llebot et al. (2013) investigated Alfacs Bay using homogeneous winds. Using spatially variable winds likely does not significantly change the circulation pattern obtained in the mentioned contributions; however their influence may be relevant in particular cases when the hydrodynamics are linked to ecological issues. Although not all these locations present similar wind variability to what we observed in Alfacs Bay, we think that proper sensitivity tests may conclude with significant differences and reveal variability in water exchanges between the semi-enclosed water body and open sea. The variability of the shape and dimensions of the coastal embayment influences the relative importance of wind variability effects, so further combined numerical and observational efforts are desirable to describe the hydrodynamics in coastal areas. Moreover, these results could be useful to understand wind variability effects on similar coastal areas with strong variability in cross-shore winds (Raubenheimer et al., 2013) and also exportable to different environments like mountain lakes, which are usually surrounded by irregular orography (Venalainen et al., 2003; Podsetchine et al., 1999).

The effects of cross-shore wind variability over the water exchange time influence the grade of the water flushing, which, in turn, controls relevant issues of the ecological behavior of the bay. For instance, in Alfacs Bay, the water flushing influences the ecological behavior of the system, determining the development of harmful algal blooms (HABs) (Loureiro et al., 2009), production of mollusk farms (Galimany et al., 2011) and fisheries, and importing/exporting species from the open sea into/out of the bay (as observed in Delgado, 1989). Further investigations linking the variability of the water exchange and the ecological evolution will benefit the sustainable management of the bay. Additional wave momentum flux due to wave height gradients is expected to be small; however, as a future work, a coupled numerical model implementation may provide a range of these forcing mechanisms.

5. CONCLUSIONS

Hydrodynamic response in coastal embayments is demonstrated to be very sensitive to wind variability. A semi-enclosed bay in the Mediterranean Sea is chosen as the application site. The wind in the bay is affected by regional and local surrounding orography. Due to the lack of high-spatial-resolution observational data, a meteorological model is used to explain the main wind patterns and to investigate the surface current response. The hydrodynamic model, ROMS, is validated against observational data, showing good skill assessment in variables such sea level, currents, and temperature, while larger errors are found in salinity. A barotropic mode of the numerical model, due

to well-mixed conditions in the bay during most extreme winter events, is used in a set of twin experiments, using winds from the WRF3 model and comparing them with spatially homogeneous wind fields. Results show the development of anti-cyclonic structures near the bay's mouth, which are related to the variation of net flows through the inner bay. A set of idealized numerical tests confirms the dependency of these hydrodynamic structures on the wind curl (vorticity). At longer timescales, the variability in hydrodynamic patterns linked to the cross-shore wind heterogeneity implies noticeable variation in associated water exchange times (20%) over some areas of the bay; this probably affects the O_2 distribution and other key ecological parameters of the bay. Comparison with a coarser meteorological model (9km) demonstrates the information lost using coarse temporal and spatial resolutions. Our results demonstrate how the spatial variability of crosswinds could notably modify the circulation patterns. These results are applicable to similar coastal areas such as harbors, bays and estuaries affected by local or regional wind variability, and they confirm the importance of spatial wind variability even in small domains.

APPENDIX

Correlation factor quantifies the strength of a linear relationship between two variables, and are defined as standardized covariance. Values close to one indicates strong linear correlation (positive or negative depending on the sign), while 0 indicates no linear relationship.

$$r(o,m) = \frac{\sum_{i=1}^{n}(m_i - \bar{m}) \cdot (o_i - \bar{o})}{n \cdot STD_o \cdot STD_m} \qquad \text{A.1}$$

In all formulas *o* represents observational data, *m* modelling results and *n* for the total amount of observational data used, and the over bar (—) denotes all data length mean values

The skill score described on Warner (2005) is defined as:

$$SK = 1 - \frac{\sum_{i=1}^{n}(m_i - o_i)^2}{\sum_{i=1}^{n}(|m_i - \bar{o}| + |o_i - \bar{o}|)^2} \qquad \text{A.2}$$

In this case values close to one indicates good agreement and equal to 0 indicates complete disagreement.

The cost function (χ) is described in (Holt et al., 2005) as:

$$\chi^2 = \frac{1}{n \cdot \sigma_o^2} \sum_{i=1}^{n} (m_i - o_i)^2 \qquad \text{A.3}$$

Where σ_o^2 is the variance of observations (square of standard deviation).

The statistics used in Normalized Taylor Diagram are normalized standard deviation:

$$\mathrm{STD}_{(m,o)} = \frac{\left(\sqrt{\frac{\sum_{i=1}^{n}(m_i - \bar{m})^2}{n}}\right)}{\sigma_o} \qquad \text{A.4}$$

And normalized root mean square error:

$$\mathrm{CRMSE}(m,o) = \frac{\sqrt{\frac{\sum_{i=1}^{n}[(o_i - \bar{o}) - (m_i - \bar{m})]^2}{n}}}{\sigma_o} \qquad \text{A.5}$$

ACKNOWLEDGMENTS

We want to thank to Joan Puigdefàbregas, Jordi Cateura and Joaquim Sospedra from Laboratori d'Enginyeria Marítima (LIM-UPC) for all their help with campaigns and data analysis, and the XIOM network (www.xiom.cat) for the information provided. We are also indebted with staff from Servei Meteorlogic de Catalunya (Meteocat) who shared with us all the atmospheric modelling data. This work was supported by a FPI-UPC pre-doctoral fellowship from the European project FIELD_AC (FP7-SPACE- 2009-1-242284 FIELD_AC). The campaigns were carried out thanks to the MESTRAL (CTM2011-30489-C02-01). The authors also acknowledge the economical funding and support received from the MINECO and FEDER who founded the Plan-Wave (CTM2013-45141-R) and Rises-AM (contract GA603396, founded by European Community's Seventh Framework programme) projects. We also want to thank to Secretaria d'Universitats i Recerca del Dpt. d'Economia i Coneixement de la Generalitat de Catalunya (Ref 2014SGR1253) who support our research group. The comments from the editor (Professor Hans Burchard) and three anonymous reviewers are appreciated

Bibliography

Alekseenko, E., Roux, B., Sukhinov, a., Kotarba, R., & Fougere, D. 2013. Nonlinear hydrodynamics in a Mediterranean lagoon. Nonlinear Processes in Geophysics, 20(2), 189–198. doi:10.5194/npg-20-189-2013

Boegman L. 2009. Currents in Stratified Water Bodies 2: Internal Waves. In: Gene E. Likens, (Editor) Encyclopedia of Inland Waters. volume 1, pp. 539-558 Oxford: Elsevier.

Bolaños, R., G. Jorda, J. Cateura, J. Lopez, J. Puigdefabregas, J. Gomez, and M. Espino. 2009. The XIOM: 20 years of a regional coastal observatory in the Spanish Catalan coast. Journal of Marine Systems 77. Elsevier B.V.: 237–260. doi:10.1016/j.jmarsys.2007.12.018.

Camp, J, and M. Delgado. 1987. Hidrografia de las bahías del delta del Ebro. Investigaciones Pesqueras 51: 351–369.

Camp, J., Romero, J., Pérez, M., Vidal, M., 1991. Production-Consumption budget in an estuarine bay: how anoxia is prevented in a forced system. Oecologia Aquat. 10, 45–56.

Camp, J. 1994. Aproximaciones a la dinámica estuarica de una bahía micromareal Mediterránea.

Carter, G.S., Merrifield, M. a., 2007. Open boundary conditions for regional tidal simulations. Ocean Model. 18, 194–209. doi:10.1016/j.ocemod.2007.04.003

Cerralbo, P., Grifoll, and M. Espino. 2015a. Hydrodynamic response in a microtidal and shallow bay under energetic wind and seiche episodes. J. Mar. Syst. 149, 1–13. doi:10.1016/j.jmarsys.2015.04.003

Cerralbo, P., M. Grifoll, J. Moré, M. Bravo, A. Sairouní Afif, and M. Espino. 2015b. Wind variability in a coastal area (Alfacs Bay , Ebro River delta). Advances in Science and Research 12: 11–21. doi:10.5194/asr-12-11-2015.

Cerralbo, P., M. Grifoll, A. Valle-Levinson, and M. Espino. 2014. Tidal transformation and resonance in a short, microtidal Mediterranean estuary (Alfacs Bay in Ebre delta). Estuarine, Coastal and Shelf Science 145. Elsevier Ltd: 57–68. doi:10.1016/j.ecss.2014.04.020.

Cerralbo, P., M. Grifoll, M. Espino, and J. López. 2012. Predictability of currents on a mesotidal estuary (Ria de Vigo, NW Iberia). Ocean Dynamics 63: 131–141. doi:10.1007/s10236-012-0586-9.

Chavanne, C., P. Flament, R. Lumpkin, B. Dousset, and A. Bentamy. 2002. Scatterometer observations of wind variations induced by oceanic islands: Implications for wind-driven ocean circulation. Canadian Journal of Remote Sensing 28: 466–474. doi:10.5589/m02-047.

Csanady, G.T. 1973. Wind induced barotropic Motions in long lakes. Journal of Physical Oceanography 3: 429–438. http://dx.doi.org/10.1175/1520-0485(1973)003<0429:WIBMIL>2.0.CO;2

Cucco, A., and G. Umgiesser. 2006. Modeling the Venice Lagoon residence time. Ecological Modelling 193: 34–51. doi:10.1016/j.ecolmodel.2005.07.043.

deCastro, M, M Gómez-Gesteira, R Prego, and R Neves. 2003. Wind influence on water exchange between the ria of Ferrol (NW Spain) and the shelf. Estuarine, Coastal and Shelf Science 56: 1055–1064. doi:10.1016/S0272-7714(02)00302-5.

Delgado, M. 1989. Abundance and Distribution of Microphytobentjhos in the Bays of Ebro Delta (Spain). Estuarine, Coastal and Shelf Science 29: 183–194. doi:10.1016/0272-7714(89)90007-3.

636 Espino, M., A.S Arcilla, and M.A. Garcıa. 1998. Wind-induced mesoscale circulation off the Ebro
637 delta, NW Mediterranean : a numerical study. Journal of Marine Systems 16: 235–251.

638 Ferrarin, C., Umgiesser, G., Bajo, M., Bellafiore, D., De Pascalis, F., Ghezzo, M., and I. Scroccaro.
639 2010. Hydraulic zonation of the lagoons of Marano and Grado, Italy. A modelling approach. Estuarine, Coastal
640 and Shelf Science, 87(4), 561–572. doi:10.1016/j.ecss.2010.02.012

641 Galimany, E., M. Ramón, and I. Ibarrola. 2011. Feeding behavior of the mussel Mytilus
642 galloprovincialis (L.) in a Mediterranean estuary: A field study. Aquaculture 314: 236–243.
643 doi:10.1016/j.aquaculture.2011.01.035.

644 Grifoll, M., Jordà, G., Espino, M., Romo, J., and M. García-Sotillo. 2011. A management system for
645 accidental water pollution risk in a harbour: The Barcelona case study. Journal of Marine Systems, 88(1), 60–
646 73. doi:10.1016/j.jmarsys.2011.02.014

647 Grifoll, M., Aretxabaleta, A.L., Pelegrí, J.L., Espino, M., Warner, John C., and A. Sánchez-Arcilla.
648 2013. Seasonal circulation over the Catalan inner-shelf (northwest Mediterranean Sea). Journal of Geophysical
649 Research: Oceans 118: 5844–5857. doi:10.1002/jgrc.20403.

650 Grifoll, M., Jordà, G., Sotillo, M.G., Ferrer, L., Espino, M., Sánchez-Arcilla, A. and E. Álvarez-Fanjul.
651 2012. Water circulation forecasting in Spanish harbours. Scientia Marina 76: 45–61.
652 doi:10.3989/scimar.03606.18B.

653 Herrera, J.L., S. Piedracoba, R.a. Varela, and G. Rosón. 2005. Spatial analysis of the wind field on the
654 western coast of Galicia (NW Spain) from in situ measurements. Continental Shelf Research 25: 1728–1748.
655 doi:10.1016/j.csr.2005.06.001.

656 Holt, J., Icarus Allen, J., Proctor, R., and Francis Gilbert. 2005. Error quantification of a high-
657 resolution coupled hydrodynamic–ecosystem coastal–ocean model: Part 1 model overview and assessment of
658 the hydrodynamics. Journal of Marine Systems 57: 167–188. doi:10.1016/j.jmarsys.2005.04.008.

659 Jiang, H., Farrar, J.T., Beardsley, R.C., Chen, R., and C. Chen. 2009. Zonal surface wind jets across
660 the Red Sea due to mountain gap forcing along both sides of the Red Sea. Geophysical Research Letters 36:
661 L19605. doi:10.1029/2009GL040008.

662 Jickells, T.D., 1998. Nutrient biogeochemistry of the coastal zone. Science 281, 217– 222

663 Jouon, A., Douillet, P., Ouillon, S., and P. Fraunié. 2006. Calculations of hydrodynamic time
664 parameters in a semi-opened coastal zone using a 3D hydrodynamic model. Cont. Shelf Res. 26, 1395–1415.
665 doi:10.1016/j.csr.2005.11.014

666 Junker, T., Schmidt, M. and V. Mohrholz. 2015. The relation of wind stress curl and meridional
667 transport in the Benguela upwelling system. Journal of Marine Systems 143. Elsevier B.V.: 1–6.
668 doi:10.1016/j.jmarsys.2014.10.006.

669 Klaić, Z. B., Z. Pasarić, G. Beg Paklar, and P. Oddo. 2011. Coastal sea responses to atmospheric
670 forcings at two different resolutions. Ocean Science 7: 521–532. doi:10.5194/os-7-521-2011.

671 Llebot, C., Rueda, F.J., Solé, J., Artigas, M.L. and M. Estrada. 2013. Hydrodynamic states in a wind-
672 driven microtidal estuary (Alfacs Bay). Journal of Sea Research. Elsevier B.V.
673 doi:10.1016/j.seares.2013.05.010.

674 Loureiro, S., Garcés, E., Fernández-Tejedor, M., Vaqué, D. and J. Camp. 2009. Pseudo-nitzschia spp.
675 (Bacillariophyceae) and dissolved organic matter (DOM) dynamics in the Ebro Delta (Alfacs Bay, NW
676 Mediterranean Sea). Estuarine, Coastal and Shelf Science 83: 539–549. doi:10.1016/j.ecss.2009.04.029.

677 Mellor, G. L. and Yamada, T., 1982: Development of a turbulence closure model for geophysical fluid
678 problems. Rev. Geophys. Space Phys., 20, 851-875.

679 Mestres, M., Sierra, J. P., and A. Sánchez-arcilla. 2007. Baroclinic and wind-induced circulation in
680 Tarragona harbour (northeastern Spain). Scientia Marina, 71(June), 223–238.

681 Narváez, D.A., and A. Valle-Levinson. 2008. Transverse structure of wind-driven flow at the entrance
682 to an estuary: Nansemond River. Journal of Geophysical Research: Oceans, 113(9), 1–9.
683 doi:10.1029/2008JC004770

684 Palacin, C., Martin, D., Gili, J.M., 1991. Features of spatial distribution of benthic infauna in a
685 Mediterranean shallow water bay. Mar. Biol. 110, 315–321. doi:10.1007/BF01313718

686 Podsetchine, V., and G. Schernewski. 1999. The influence of spatial wind inhomogeneity on flow
687 patterns in a small lake. Water Resources Research 33: 3348–3356.

688 Pritchard, D. W. 1952. Estuarine Hydrography. Advances in Geophysics, Volume 1. Edited by H. E.
689 Landsberg, Geophysics Research Directorate, Air Force Cambridge Research Center. Published by Academic
690 Press, Inc., New York, USA, 1952, p.243

691 Raubenheimer, B., Ralston, D.K., Elgar, S., Giffen, D., Signell, R.P., 2013. Observations and pre-
692 dictions of summertime winds on the Skagit tidal flats, Washington. Cont. Shelf Res. 60, 1–9.
693 doi:10.1016/j.csr.2012.02.001

694 Rueda, F., Vidal, J. and G. Schladow. 2009. Modeling the effect of size reduction on the stratification
695 of a large wind-driven lake using an uncertainty-based approach. Water Resources Research 45: 1–15.
696 doi:10.1029/2008WR006988.

697 Schaeffer, A., Garreau, P., Molcard, A., Fraunié, P., and Y. Seity. 2011. Influence of high-resolution
698 wind forcing on hydrodynamic modeling of the Gulf of Lions. Ocean Dynamics 61: 1823–1844.
699 doi:10.1007/s10236-011-0442-3.

700 Schoen, J., Stretch, D. and K. Tirok. 2014. Wind-Driven circulation patterns in a shallow estuarine
701 lake: St Lucia, South Africa. Estuarine, Coastal and Shelf Science. doi:10.1016/j.ecss.2014.05.007.

702 Shchepetkin, A.F., and J.C. McWilliams. 2005. The regional oceanic modeling system (ROMS): a
703 split-explicit, free-surface, topography-following-coordinate oceanic model. Ocean Modelling 9: 347–404.
704 doi:10.1016/j.ocemod.2004.08.002.

705 Signell, R.P., Carniel, S., Cavaleri, L., Chiggiato, J., Doyle, J.D., Pullen, J. and M. Sclavo. 2005.
706 Assessment of wind quality for oceanographic modelling in semi-enclosed basins. Journal of Marine Systems
707 53: 217–233. doi:10.1016/j.jmarsys.2004.03.006.

708 Skamarock, W. C., Klemp, J.B., Dudhia, J., Gill, D.O., Barker, D.M., Duda, M., Huang, X.-Y., Wang,
709 W. and Powers, J.G. NCAR Technical Note, 2008

710 Taylor, K.E. 2001. Summarizing multiple aspects of model performance in a single diagram. Journal
711 of Geophysical Research 106: 7183–7192.

712 Tonani, M., Pinardi, N., Fratianni, C., Pistoia, J., Dobricic, S., Pensieri, S., M De Alfonso, and K Nittis.
713 2009. Mediterranean Forecasting System : forecast and analysis assessment through skill scores. Ocean
714 Science: 649–660.

715 Valle-levinson, A., and L.Blanco. 2004. Observations of wind influence on exchange flows in a strait
716 of the Chilean Inland Sea. Journal of Marine Research 62: 721–741.

717 Venäläinen, A., Sahlgren, V., Podsechin, V., Huttula, T., 2003. Small-scale variability of the wind fi
718 eld over a typical Scandinavian lake. Boreal Environ. Res. 8, 71–81.

719 Warner, J. C., Sherwood, C. R., Arango, H. G., and R.P. Signell. 2005. Performance of four turbulence
720 closure models implemented using a generic length scale method. Ocean Modelling, 8(1-2), 81–113.
721 doi:10.1016/j.ocemod.2003.12.003

722 Warner, J.C., 2005. Numerical modeling of an estuary: A comprehensive skill assessment. J. Geophys.
723 Res. 110, 1–13. doi:10.1029/2004JC002691

724 Wilmott CJ. 1981. On the validation of models. Phys Geogr 2:184–194

725 Wolanski, E. 2007. Estuarine Ecohydrology. Elsevier. 157pp. ISBN: 978-0-444-53066-0

726 Wong, K.-C. 1994. On the nature of transverse variability in a coastal plain estuary, J. Geophys. Res.,
727 99 (C7), 14209–14222, doi:10.1029/94JC00861.

728 Zampato, L., Umgiesser, G. and S. Zecchetto. 2007. Sea level forecasting in Venice through high
729 resolution meteorological fields. Estuarine, Coastal and Shelf Science 75: 223–235.
730 doi:10.1016/j.ecss.2007.02.024.

731